Development at the University of North Dakota of a Digital Thermosonde Instrument for the Study of Atmospheric Optical Turbulence (C_n^2)

Blake T. Sorenson[*a], *James Casler*[b], *and David J. Delene*[a]

[a]*Department of Atmospheric Sciences, University of North Dakota, Grand Forks, ND*
[b]*Department of Space Studies, University of North Dakota, Grand Forks, ND*

*Students: blake.sorenson@und.edu**
Mentor: james.casler@und.edu david.delene@und.edu

ABSTRACT
Atmospheric optical turbulence affects the transmission of electromagnetic waves between the Earth's surface and space. High optical turbulence results in noisier ground to satellite communication and degraded satellite images. Earth surface images obtained from satellites, and stellar object images from ground telescopes, are enhanced greatly when accounting for optical turbulence in real time. To study optical turbulence profiles, a NASA Undergraduate Student Instrument Project (USIP) at the University of North Dakota (UND) constructed a balloon-borne, digital thermosonde that measures high-resolution temperature differences using a fine-wire platinum thermocouple. The USIP team used a design based on work done by NASA in the 1970s and improved on by the Air Force Research Laboratory (AFGL). Two tethered balloon flights indicate that the thermosonde measured temperature difference agrees with the lower end of the expected temperature differences derived from National Weather Service sounding data. Similar refractive index structure parameter profiles are obtained from Graw radiosondes temperature measurements and the thermosonde horizontal temperature differences measurements, which are consistent with previous studies. The USIP team demonstrated that undergraduate students can successfully build a thermosonde system based on the NASA/AFGL design and deploy the thermosonde system to obtain optical turbulence measurements.

KEYWORDS
Optical turbulence; refractive index structure parameter; thermosonde; radiosonde; ballooning; airborne measurements; vertical profile

INTRODUCTION
Temperature differences, particulate matter, and precipitation distort wireless communications through the Earth's atmosphere.[1] Differences in atmospheric temperature affect the transmission of electromagnetic signals, including visible light. Just as light passing from air into water causes underwater objects to appear distorted, atmospheric layers of different density bend light differently causing distortions. Larger differences in layer density result in higher image distortion and increased noise for communication signals. For laser systems, density variations cause beam steering, image dancing, and beam spreading, which affect image and communication quality.[2] Atmospheric optical turbulence is defined as the distortion of light passing through the atmosphere caused by layers with differing density. Density differences cause optical turbulence mainly due to temperature and humidity variations. Temperature variations are important throughout the troposphere, while humidity variations are primarily important in the planetary boundary layer since water vapor content above the planetary boundary layer is typically low and thus has little effect on density variations.

Commented [DD1]: Remove "images" since it does not require making an image, the objective will always naturally appear distorted. Some telescope system can create images that are "correct" for the effect and hence not necessary that all image are distorted.

Optical turbulence research dates back to the early 1960s when Tatarski first proposed a relationship between density and turbulence.[3] Optical turbulence is usually quantified by the refractive index structure parameter, C_n^2, and can be calculated using Obukhov-Kolmogorov turbulence theory, which has the temperature structure parameter given by

$$C_T{}^2(h) = \left\{\frac{[T(d_1) - T(d_2)]^2}{d^{\frac{2}{3}}}\right\}, \qquad \textbf{Equation 1.}$$

where $\mathrm{T(d_1)}$ and $\mathrm{T(d_2)}$ are high-resolution horizontal temperature measurements and $d = |d_2 - d_1|$ is the distance between two temperature measurements.[4,5] C_n^2 is related to C_T^2 by standard meteorological parameters using the Dale-Gladstone Relationship,

$$C_n^2 = (79 * 10^{-6}(\tfrac{P}{T^2}))^2 C_T^2, \qquad \textbf{Equation 2.}$$

where P is atmospheric pressure in mb and T is temperature in Kelvin.[3] We note that slight variations in this equation were found in the literature; while some studies report this equation using the form of 79×10^{-6},[7,11,12] others report the equation using 80×10^{-6}.[6] Nevertheless, since we found more studies referring to the equation with the coefficient as 79, we use 79 in this study.

Formatted: Superscript

Formatted: Superscript

Formatted: Font: Not Bold

The thermosonde, an instrument that measures temperature differences, was developed in the late 1960s and early 1970s. The thermosonde uses two 2 µm diameter platinum wires spaced one meter apart to measure temperature difference.[6] The first balloon-borne temperature difference profiles showed that areas of high optical turbulence are confined to the surface boundary layer, the lower troposphere, and the tropopause. The layers corresponded to areas of high wind shear and temperature inversions.

The refractive index structure parameter can be determined using temperature differences from atmospheric models. The Air Force Geophysical Lab (now the Air Force Research Laboratory) developed the Dewan model, which has become one of the more widely used models for calculating the refractive index structure parameter. The Dewan (AFGL) model defines optical turbulence using:

$$C_n^2 = 2.8[(\frac{79\times10^{-6}P}{T^2})(\frac{\partial T}{\partial z}+\gamma)]^2(0.1)^{4/3}10^{Y(z)}, \quad \textbf{Equation 3.}$$

where

$$Y(z) = 1.64 + 42.0 \times S_{raw} \textbf{ (Troposphere)} \quad \textbf{Equation 4.}$$

$$Y(z) = 0.506 + 50.0 \times S_{raw} \textbf{ (Stratosphere)} \quad \textbf{Equation 5.}$$

and

$$S_{raw} = \sqrt{\frac{\partial u^2}{\partial z} + \frac{\partial v^2}{\partial z}} \quad \textbf{Equation 6.}$$

where P is atmospheric pressure in mb, T is temperature in Kelvin, γ is the dry adiabatic lapse rate, u is the zonal wind component, and v is the meridional wind component.[7] Other optical turbulence-estimating models have been developed to estimate the refractive index structure parameter from standard meteorological profile data, including the Hufnagel and Van Zandt models,[8,9] but a comparison study indicated that between the Hufnagel, Van Zandt, and AFGL models, the AFGL model outperformed the others at estimating the refractive index structure parameter.[7] Due to the complexity of modeling boundary layer turbulence, the AFGL model is not valid for the boundary layer. The AFGL model does not account for moisture-induced density fluctuations; therefore, the model is more suitable for the drier atmosphere above the boundary layer.[7] Hence, only measurements above 3 km (maximum boundary layer height) are analyzed using the AFGL model. A thermosonde measurement of C_n^2 has been compared to the high-resolution Weather Research and Forecasting (WRF) model, with logarithmic differences between the radiosonde-estimated C_n^2 and the WRF forecasts of ${C_n}^2$ found to be 0.090 ± 0.823.[11] A potential source of error with using the platinum-wire thermosonde is the impact of solar heating. Richardson found that solar heating of the 4.7 µm diameter platinum-coated tungsten wires could cause errors of two orders of magnitude on C_n^2 measurements.[10] To reduce the impact of solar heating, thinner wires made of more reflective and thermally smooth metals such as pure platinum, silver, or aluminum can be used.[10]

METHODS

The digital thermosonde is based on the Air Force Research Laboratory designs from the 1970s, which has been used in various projects over the last 50 years.[6,12] The thermosonde measures temperature difference using two 2 µm diameter platinum wire probes (Figure 1~~Figure 1~~). The temperature probe is two arms of an unbalanced Wheatstone Bridge that provides the 1 m temperature difference measurement as a voltage difference. The voltage difference is amplified, conditioned, and converted to an analog signal representing the root mean square of the voltage difference, which is measured by a high precision analog-to-digital board and stored locally on a Secure Digital (SD) card and sent to the ground using the XDATA protocol of the Graw radiosonde. XDATA is a standard protocol for chaining together data from multiple instruments into the radiosonde's data stream.[13] Graw DFM-09 radiosondes (white probe in Figure 1~~Figure 1~~) measures the standard meteorological parameters of pressure, temperature, wind, and altitude. The radiosonde sends data to a ground receiving station at 24 bps.

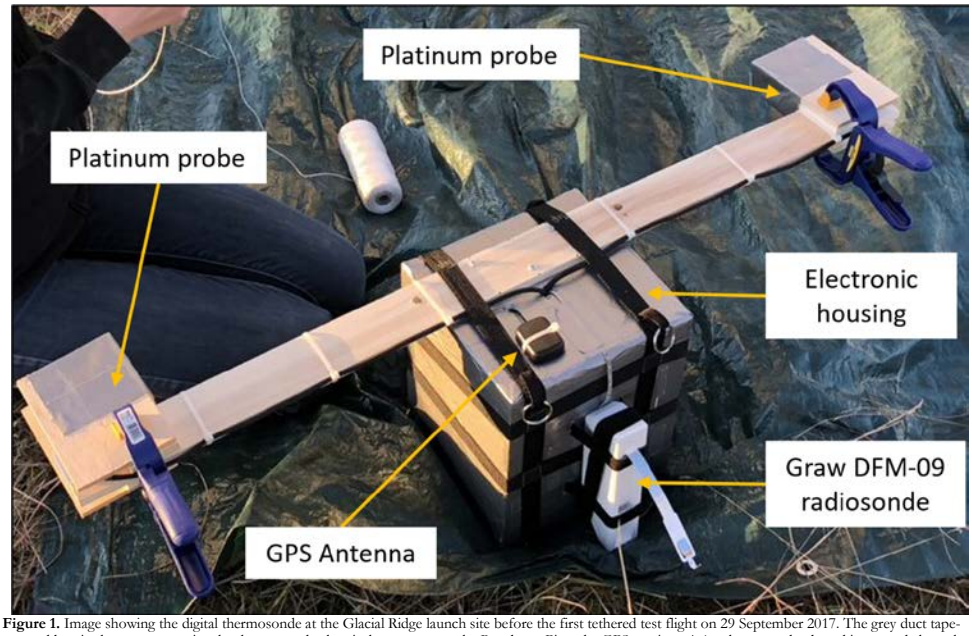

Figure 1. Image showing the digital thermosonde at the Glacial Ridge launch site before the first tethered test flight on 29 September 2017. The grey duct tape-covered box in the center contains the thermosonde electrical components, the Raspberry Pi, and a GPS receiver. A 1 m long wooden board is secured along the Styrofoam box with two daughter boards at the board ends that contain the 2 μm diameter platinum wire probes. A shield made from two wood blocks is secured around the probes until launch to prevent probe damage during balloon systems preparation.

The thermosonde is part of a balloon package system (Figure 2~~Figure 2~~) that records voltage difference throughout a typical 2.5 hr flight, which includes both balloon ascent and descent after balloon burst. To minimize thermal wake effects caused by the balloon's ascent, the thermosonde is suspended in a harness 55 meters below the balloon.[14] The Raspberry Pi inside the thermosonde sends voltage difference data to the radiosonde, which transmits the data to the ground station along with radiosonde data. The ground station uses a Graw omnidirectional antenna mounted vertically a few feet above ground level to receive the data using a laptop and the Grawmet sounding software. The voltage difference measurements are stored in raw data files (.gsf file extension), while the radiosonde measurements are saved as text files.

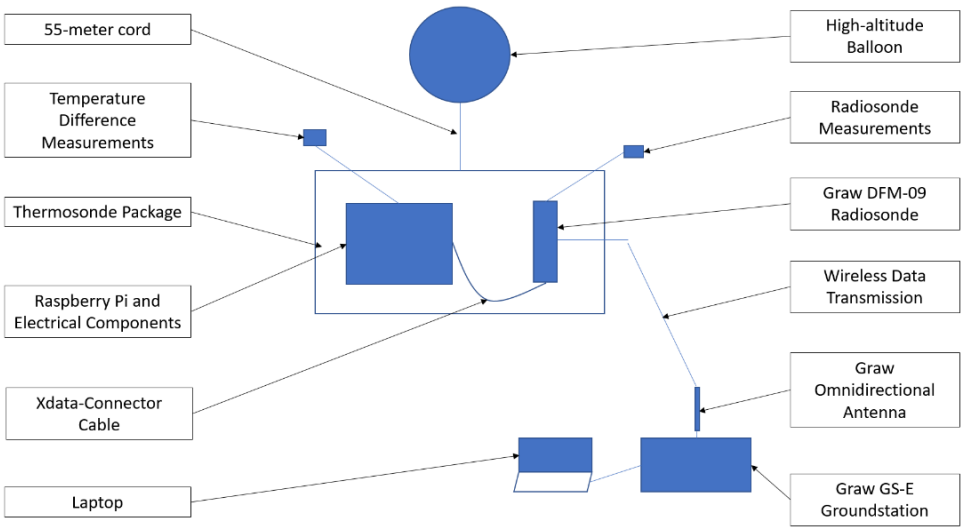

Figure 2. Block diagram (not to scale) showing the balloon package components and the data transferred through the system. The Thermosonde voltage difference measurement is sent from the Raspberry Pi to the Graw radiosonde (DFM-09) using the radiosonde's XDATA cable. The voltage difference data are transmitted to the ground station along with radiosonde data.

The thermosonde voltage representing the temperature difference includes noise that results in an approximately 0.23 V offset. The voltage offset must be addressed to ensure the voltage represents a true temperature difference. To determine the voltage offset, data from a 11 November 2017 test flight are analyzed, in which the thermosonde is attached to a tether balloon system and flown to approximately 500 ft above ground level. The test flight data are used to correct the thermosonde's voltage measurements by determining relationships between the raw voltage measurements and the corrected voltages. For root mean square voltages less than 0.66 V, the relation between the raw and corrected voltages (Figure 3~~Figure 3~~**a**) is logarithmic, while the relationship is linear for voltages larger than 0.66 V. These relations are given by the following equations,

$$V_{corrected} = 0.553 * ln(V_{rms}) + 0.844 \, , for \, V_{rms} \leq 0.66 \, V \qquad \textbf{Equation 7.}$$

$$V_{corrected} = 1.019 * V_{rms} - 0.048 \qquad , for \, V_{rms} > 0.66 \, V \qquad \textbf{Equation 8.}$$

where $V_{corrected}$ is the corrected voltage accounting for the instrument noise floor and V_{rms} is the raw root mean square (RMS) voltage measured by the thermosonde, with the root mean square voltage being the square root of the mean square of the instantaneous voltage values sampled by the sensor. The RMS voltage can also be described as the amount of alternating current (AC) power drawn from a resistor similar to the power drawn by a direct current (DC). The corrected voltages are converted to temperature difference using a linear equation given by,

$$\Delta T = 0.129 V_{corrected} \qquad \textbf{Equation 9.}$$

where $V_{corrected}$ is the thermosonde voltage calculated with the calibration equations given by Equation 7~~Equation 7~~ and Equation 8~~Equation 8~~. Unlike the voltage relationship, which is logarithmic for smaller voltages and linear for larger voltages, the relation between the corrected voltage and temperature differences (Figure 3~~Figure 3~~**b**) is linear for all voltages.

Formatted: Book Title,EquationTable

Formatted: Book Title,EquationTable

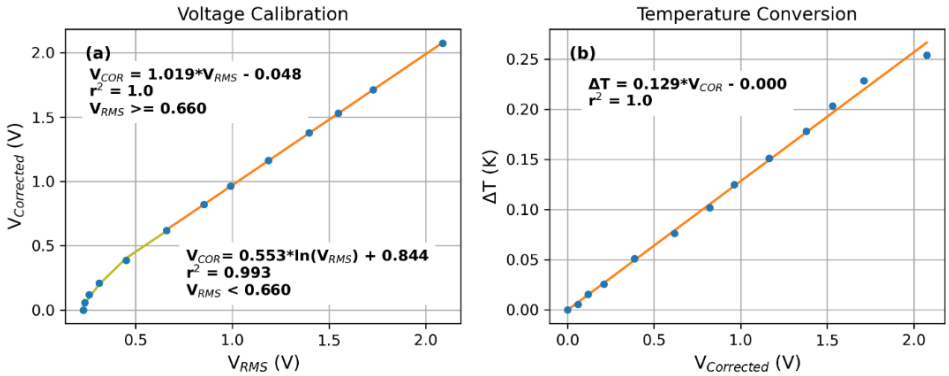

Figure 3. (a, left) The relationship) between the root mean square voltage (V_{rms}) measured by the thermosonde and the corrected voltage ($V_{corrected}$) using data from the Glacial Ridge field site on 17 November 2017. (b, right) The relation between the corrected voltage ($V_{corrected}$) on the thermosonde's Wheatstone bridge and the temperature difference measured by the platinum-wire probes (ΔT).

In addition to the measured thermosonde C_n^2 profiles, C_n^2 is calculated by using the radiosonde measurements and by using High-resolution Rapid Refresh (HRRR) model data. The HRRR model sounding data are obtained from the NOAA Air Resources Laboratory (ARL) Archived Meteorology database (https://www.ready.noaa.gov/READYamet.php) at the latitude and longitude of the thermosonde launch site. The HRRR soundings have 3 km horizontal grid spacing and roughly 50 vertical levels; therefore, the radiosonde and thermosonde profiles have much higher vertical resolution than the HRRR profile. Hence, the radiosonde and thermosonde data are averaged to match the vertical resolution of the model profile for comparison. All data from a thermosonde launch are processed to extract voltage measurements from the xml-formatted Graw files. Profiles of the refractive index structure parameter are calculated for the thermosonde, radiosonde and model data. All programs used for data analysis are part of the open-source Airborne Data Processing and Analysis (ADPAA) software package.[15]

To collect measurements for calculating the refractive index structure parameter, the thermosonde system was launched from the UND Glacial Ridge Atmospheric Observatory southeast of Crookston, Minnesota and from Mayville State University in Mayville, North Dakota. The long (55 m) suspension line for the thermosonde creates issues that are not present during a balloon launch in which the package is located close to the balloon. Even an experienced launch team needs to understand and review these differences to ensure a safe and successful launch. Enough area is required to lay out the line between the balloon and package. The balloon needs to lift the package high enough to clear any obstructions around the launch site. The main obstructions at the Glacial Ridge site are power lines on the west side of the site and a fence around the trailer and wind profiler (Figure 4~~Figure 4~~) The 5 May 2018 launch had an easterly wind; therefore, the balloon is positioned on the east side and the line strung out to the west so the balloon rises above the line when released. Depending on the wind speed, people holding the line and package need to move towards the balloon to allow the line and package to be lifted straight up out of their hands. Having the line and package lifted straight up ensures that package is not dragged along the ground, which could damage sensors. Additionally, there needs to be enough "Clearance Distance" to ensure that the package does not hit any obstructions. The power line obstruction is 10.4 m (34 ft) above ground and the maximum allowed wind speed for a launch is 6.7 m/s (15 mile per hour); therefore, a "Clearance Distance" of 25.7 m (or 3.84 s) is required, assuming a 2.7 m/s (530 ft/min) ascent rate. Hence, the balloon needs to be a total of 80.7 m (25.7 + 55 m) from the power line for an easterly wind. A tarp is useful for laying out the suspension line and an anchor helps so people do not have to hold the balloon when attaching the thermosonde package. It can be difficult to hold the balloon on a cold night, especially if there is a delay in getting the thermosonde package ready. Sufficient helium is added to the balloon to have a raise rate of approximately 5 m s^{-1}. This 5 m s^{-1} ascent and the thermosonde's 5 Hz data sampling rate results in a vertical measurement resolution of 1 m.

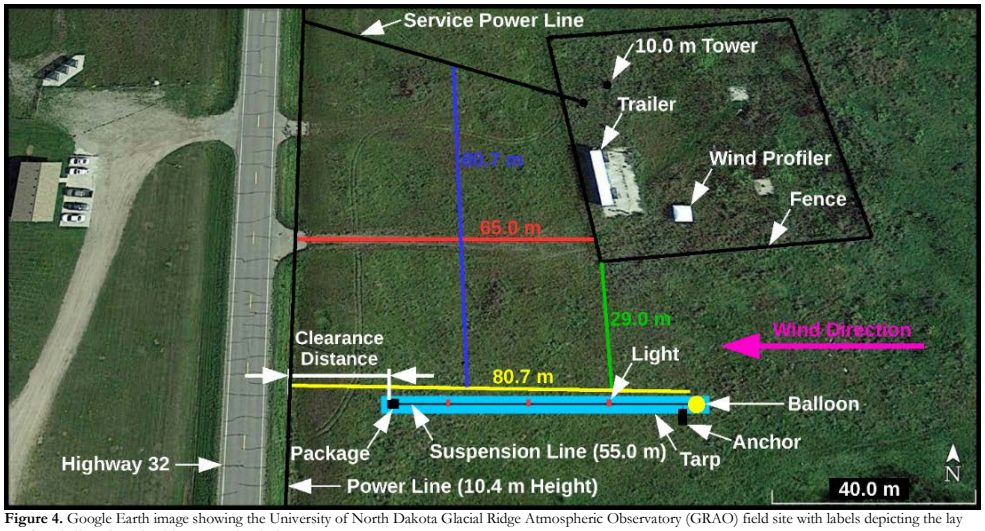

Figure 4. Google Earth image showing the University of North Dakota Glacial Ridge Atmospheric Observatory (GRAO) field site with labels depicting the lay out for a balloon launch with an easterly wind.

RESULTS

A) 5 May 2018 Balloon Flight

A night launch of the thermosonde was conducted starting 4 May and ending 5 May 2018. Compared to daytime, a night profile has reduced thermal turbulence caused by the balloon.[11] During the day, the latex balloon is warmed by the sun as the balloon ascends. Air in contact with the warm balloon surface also warms resulting in warmed air being pulled into the balloon's turbulent wake causing additional turbulence below the balloon. Suspending the thermosonde 50 m below the balloon does minimize this balloon's wake effect. During the flight, the thermosonde ascended at 5 m s^{-1} to an altitude of 28 km where the balloon bursts and the package descended to the surface and was recovered.

~~After analyzing the~~The ~~time series of the~~ raw thermosonde voltages obtained during the flight indicated an instrument noise floor of 0.2 V, which is used to postprocess the voltage data. The raw voltages are corrected to account for the instrument noise floor using the equations:

$$V_{corrected} = 0.4696 * ln(V_{rms}) + 0.7847 \, , for \; V_{rms} \leq 0.436 \, V \qquad \textbf{Equation 10.}$$

$$V_{corrected} = 1.0206 * V_{rms} - 0.046 \qquad , for \; V_{rms} > 0.436 \, V \qquad \textbf{Equation 11.}$$

The corrected voltages are applied to **Equation 9** to obtain the temperature difference values, which are used with the radiosonde-measured meteorological variables to calculate C_n^2. **Figure 5**~~The time series of thermosonde temperature differences obtained during the thermosonde flight are shown in **Figure 5**. To determine the validity of the thermosonde measurements before calculating C_n^2, the thermosonde temperature differences are compared to the vertical temperature differences measured by the radiosonde. Both the Graw radiosonde and the thermosonde sample at 1 Hz; hence, the temperature differences can easily be temporally matched. The radiosonde vertical temperature difference is found by dividing the difference in temperature between each radiosonde measurement by the difference in altitude between each measurement. The precision of the radiosonde (0.1 K) is much lower than the thermosonde (0.001 K); therefore, this comparison is meant to confirm that the temperature differences measured by the thermosonde are generally comparable to the radiosonde temperature differences. After an initial temperature difference increase shortly after launch, the radiosonde recorded negative temperature differences through the troposphere. A very large increase in thermosonde temperature differences is located at almost the same time as the radiosonde temperature difference; therefore, the large increase is likely caused by an inversion. At approximately 21,900 seconds, the radiosonde reports positive temperature differences, which indicates the package crossing the tropopause and entering the stratosphere. Before the~~

Formatted: Normal

~~package reaches the stratosphere, the thermosonde temperature differences exhibit an increasing number of large increases that quickly stop after the package reaches the stratosphere. The mean thermosonde temperature difference value also decreases after the radiosonde begins recording positive vertical temperature difference values, which suggests that the thermosonde is resolving the turbulence around the tropopause. The absolute values of the radiosonde vertical temperature differences shown a more direct comparison of the range of differences measured by both the radiosonde and thermosonde. Aside from the time window between the two major increases in thermosonde temperature differences, the radiosonde temperature differences match up well with the thermosonde temperature differences. The radiosonde temperature differences do not exhibit the increase that the thermosonde temperature differences exhibit due to the lower precision of the radiosonde's temperature sensor, but the radiosonde values roughly agree with the average thermosonde values.~~

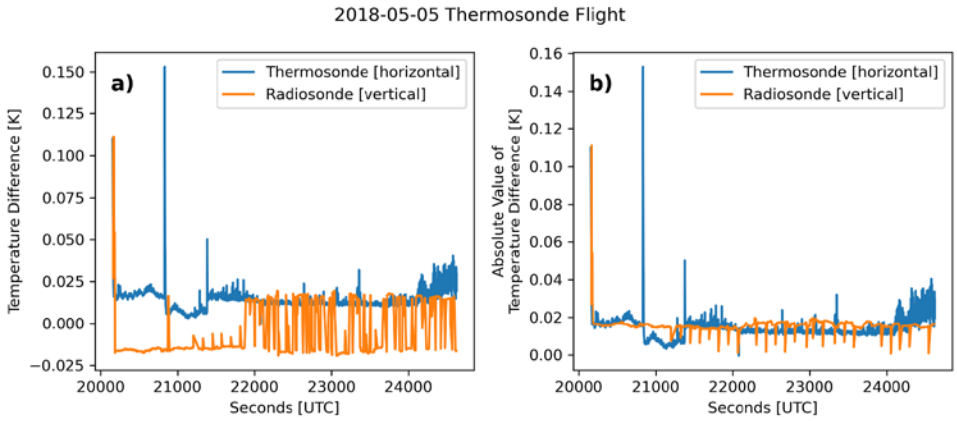

~~**Figure 5**. Comparison of the 1-m horizontal temperature differences observed by the thermosonde (blue) with the 1-m vertical temperature differences derived from the radiosonde data (a, orange) and the absolute value of the radiosonde vertical temperature differences (b, orange) from the 05Z 5 May 2018 thermosonde launch.~~

shows the meteorological and thermosonde measurements from a launch on 5 May 2018. The air temperature profile (**Figure 5a**) exhibit an inversion in the lowest 500 m, above which air temperature decreases steadily until the tropopause at an altitude of about 11 km. The radiosonde-measured wind speed (**Figure 5b,** blue) and wind direction (**Figure 5b**, orange) reveal light southeasterly winds near the surface, with the winds increasing in speed and veering to the northwest through the troposphere. Maximum wind speeds of about 60 kts were observed just below the tropopause at about 11 km, with wind speeds decreasing in the stratosphere; we note that the wind speeds exhibit considerable variability in the stratosphere. The horizontal temperature differences observed by the thermosonde (**Figure 5c**) for altitudes primarily ~~The 05Z 05 May 2018 HRRR model sounding (**Figure 6a**, red) agrees very well with the radiosonde profile (**Figure 6a**, blue). Both the radiosonde and model soundings show a strong temperature inversion at 950 mb, a small temperature inversion at approximately 550 mb (~4900 m), and a peak wind speed of 60 kts near 300 mb. **Figure 6b** shows that the temperature difference~~ lower that 4.5 km ~~is~~ are ~~approximately~~ about 0.02 K~~, with some slight variations~~. At approximately 5 km, there is a large increase up to 0.15 K, and after the increase the temperature differences drop to half of the pre-increase value. ~~The same level of variability before the increase is apparent after the increase.~~ At 9.5 km, there is another large increase, and the temperature differences increase back to around 0.02 K. ~~The increase near the surface is a valid measurement; however, the two large positive increases are likely artifacts due to the data logging software.~~ At approximately 13 km, there is a temperature difference that drops below 0 K, which is ~~also~~ likely an artifact.

Formatted: Normal, Don't keep with next

Formatted: Normal

Formatted: Font: Bold

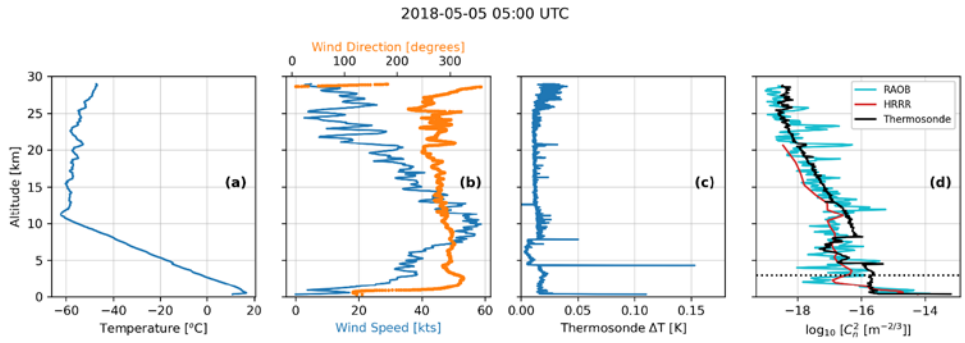

Figure 5. Data from the 05 May 2018 thermosonde launch from the Glacial Ridge Observatory near Mentor, MN. a) Air temperature observed by the radiosonde. b) Wind (blue) speed and (orange) direction observed by the radiosonde. C) Thermosonde-measured temperature differences. d) Thermosonde-calculated (black), radiosonde-estimated (blue), and model-estimated (red) C_n^2. The dashed line represents the 3 km minimum for evaluating the error between the profiles.

Using the Dewan model, estimates of C_n^2 were constructed from the radiosonde data and from a HRRR model profile centered on the site of the thermosonde package launch. Both the ~~model and~~ radiosonde- (**Figure 5d**, cyan) and HRRR-based (**Figure 5d**, red) estimates show C_n^2 values between 10^{-14} and 10^{-15} $m^{-2/3}$ in the lowest 2 km of the atmosphere, with a very sharp decrease in C_n^2 at about 3 km down to the range of 10^{-17} to 10^{-16} ~~(**Figure 6c**)~~. Due to the differences in resolution between the radiosonde data and model sounding, the radiosonde-estimated ${C_n}^2$ exhibits much more variability than the HRRR model sounding. The radiosonde profile is averaged to match the resolution of the model sounding, which enables a direct comparison of the datasets, following the methodology of Frehlich et al.[11] The radiosonde data (temperature, pressure, and u and v-wind components) are averaged around each HRRR model altitude so the vertical resolution of the radiosonde data is consistent with the HRRR profile's vertical resolution. The average of the differences of the profiles' logarithmic C_n^2 estimations is 0.005 +/- 0.159. For the troposphere, the average difference is 0.017 +/- 0.183, and for the stratosphere, the average difference is 0.024 +/- 0.073.

The temperature differences are matched to the radiosonde data ~~using the thermosonde timestamp~~, and the Dale-Gladstone Relation (~~Equation 2~~**Equation 2**) is applied to the combined data to obtain C_n^2 from the thermosonde temperature differences. The thermosonde C_n^2 (**Figure 5d,** black) and radiosonde-estimated C_n^2 (**Figure 5**~~**Figure 6d,** cyan~~) show many of the features seen in the thermosonde temperature differences (~~**Figure 6b**~~c), including the increase in thermosonde C_n^2 just below the tropopause (approximately 12 km). ~~A comparison of the thermosonde C_n^2 after averaging to match the resolution of the averaged radiosonde-estimated C_n^2 is seen in **Figure 6c**. The averaging removes several features apparent in **Figure 6b**, including the increasing thermosonde values near the tropopause.~~ For the 05 May 2018 flight, the average logarithmic C_n^2 difference between the thermosonde and radiosonde-estimated C_n^2 is 0.260 +/- 0.535. For the troposphere, the average difference is 0.058 +/- 0.628, and for the stratosphere, the average difference is 0.410 +/- 0.441. For comparison, Frehlich et al. found an average difference value of 0.065 +/- 1.236 for the troposphere and an average difference value of 0.116 +/- 0.359 for the stratosphere.[11]

Field Code Changed

Formatted: Font: Not Bold

Field Code Changed

Field Code Changed

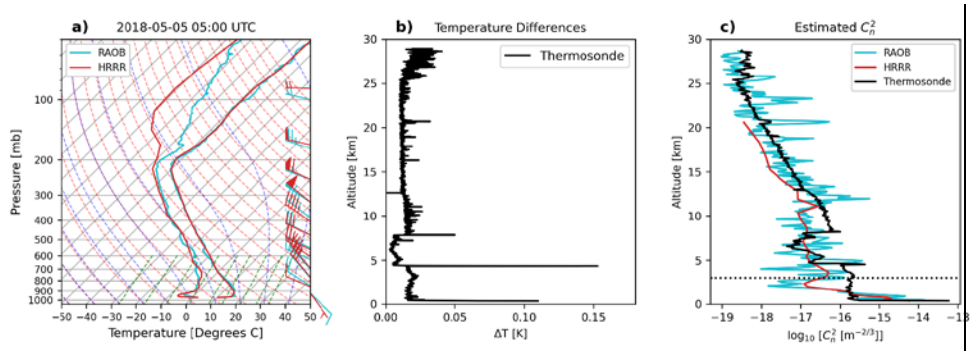

~~**Figure 6.** Data from the 05 May 2018 thermosonde launch starting at 05:11 UTC from the Glacial Ridge Observatory near Mentor, MN. a) Skew-T Log-P diagram of the Graw DFM-09 radiosonde (cyan) and the High-Resolution Rapid Refresh (HRRR) model sounding for the time and location of the launch (red). b) Thermosonde-measured temperature differences. c) Thermosonde-calculated (black), radiosonde-estimated (cyan), and model-estimated (red) C_n^2. The dotted line represents the 3 km minimum for evaluating the error between the profiles.~~

Formatted: Don't keep with next

C) 4 May 2019 Balloon Flight

A second balloon flight was conducted on 04 May 2019 at 03:00 UTC, with the launch site moved to Mayville State University in Mayville, ND. One of the main goals of the second launch is to determine if changes to the thermosonde's electronic components allow for more variability in the voltage measurements than in the 5 May 2018 launch. As with the 5 May 2018 first launch, the raw temperature difference is adjusted through the noise floor correction (Figure 6~~Figure 7~~**a**) and the temperature difference conversion (Figure 6~~Figure 7~~**b**). The resulting temperature difference values, as well as the meteorological variables from the radiosonde, are used to calculate C_n^2.

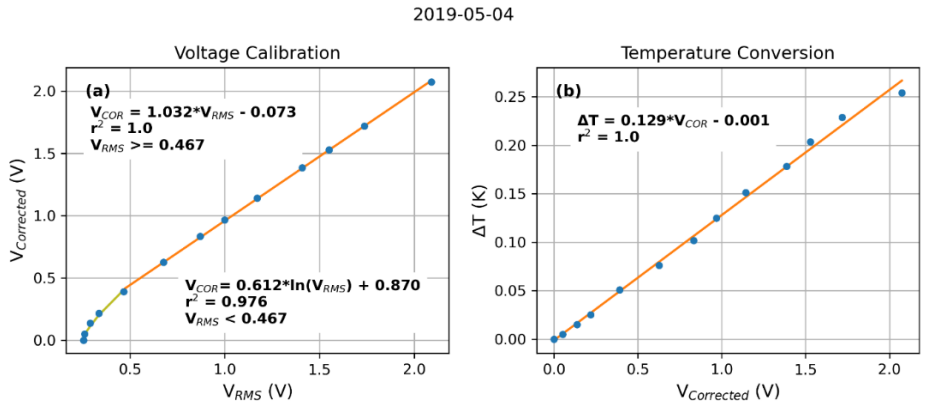

Figure 6. a) Voltage correction relations for the thermosonde data from the second thermosonde flight at 03:00 UTC 04 May 2019. b) Conversion relation between the corrected voltages and the temperature difference values.

Due to an unexpected early loss of communication with the thermosonde during the 4 May 2019 flight, data are only available for approximately the first half of the thermosonde ascent, from the surface to an altitude of approximately 6.5 km. The radiosonde ~~and HRRR model~~temperature profile~~s~~ (Figure 7~~Figure 8~~**a**) show~~s general agreement from the surface until the loss of radiosonde data~~a radiation inversion near the surface as well as a second inversion at an altitude of about 2.5 km. ~~The HRRR~~

~~profile correctly resolves the surface inversion; however, it does not resolve the capping inversion at the top of the residual boundary layer at approximately 750 mb.~~ The profiles of wind speed (**Figure 7b**, blue) and direction (**Figure 7b**, orange) show light southwesterly winds at the surface, with the winds veering to the northwest and increasing in speed to near 40 kts at 5 km. Aside from very large temperature differences within the lowest 500 m of the flight, the thermosonde temperature differences (**Figure 7c**) are primarily below 0.05 K through the flight. The temperature differences from the 4 May 2019 thermosonde flight exhibit notably higher variability than the temperature differences from the 5 May 2018 thermosonde flight, with the temperature differences from the 4 May 2019 flight repeatedly varying from near 0 to about 0.025 K between altitudes of 2 km to 6.5 km.

C_n^2 profiles estimated from the averaged radiosonde data (**Figure 7~~Figure 8c~~d**, blue) and the HRRR model sounding (**Figure 7~~Figure 8c~~d**, red) show C_n^2 values between 10^{-15} and 10^{-14} $m^{-2/3}$ near the surface, with a very sharp decrease in C_n^2 just above the surface to about 10^{-16} $m^{-2/3}$. Due to the differences in resolution between the radiosonde data and model sounding, the radiosonde-estimated C_n^2 exhibits much more variability than the HRRR model sounding. The radiosonde-estimated C_n^2 vary by several orders of magnitude between 1 km and 6 km, while the HRRR values only vary within a single order of magnitude. Due to the early termination of the radiosonde, there is limited data to calculate the comparison statistics for the profiles above 3 km. As with the 5 May 2018 flight, thermosonde C_n^2 are calculated from the temperature differences and the radiosonde meteorological measurements. ~~As shown in **Figure 8c**, b~~Both the radiosonde-estimated C_n^2 (**Figure 7d**, cyan) and the thermosonde C_n^2 (**Figure 7d**, black) exhibit variability during the ascent, with the radiosonde estimates showing larger amplitude variations than the thermosonde values. The thermosonde C_n^2 values are approximately two orders of magnitude larger than the radiosonde-estimated values at the surface, but above 1 km, both profiles oscillate around values on the order of $10^{-16.5}$. The profile stops at just over 6 km due to lost connection; therefore, the C_n^2 behavior in the upper atmosphere near the tropopause is not quantifiable. However, from the 6 km of data the thermosonde collected, strong variability in both the radiosonde-estimated and thermosonde C_n^2 is seen.

Formatted: Font: Bold

Formatted: Font: Bold

Formatted: Font: Bold

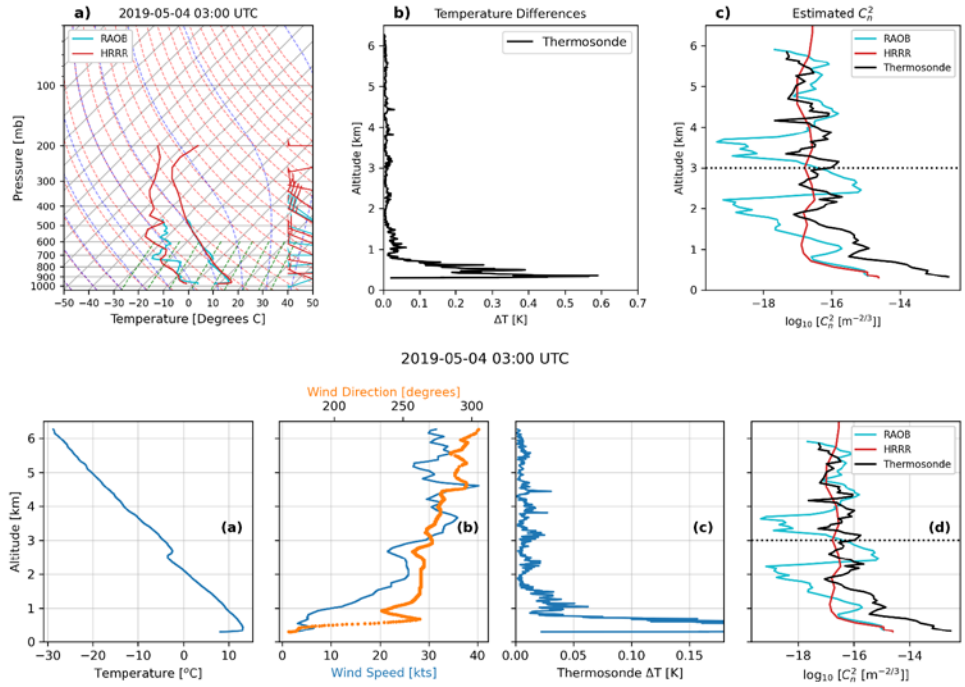

Figure 7. Data from the thermosonde launch on 04 May 2019 ~~at 03:00 UTC~~ from the Mayville State University campus in Mayville, ND. a~~)~~ ~~Skew-T Log-P diagram of the Graw DFM-09 radiosonde in the thermosonde instrument package (blue) and the High-Resolution Rapid Refresh (HRRR) model sounding for the time and location of the launch (red))~~ Air temperature observed by the radiosonde. b) Wind (blue) speed and (orange) direction observed by the radioosnde. C) Thermosonde-measured temperature differences. ~~e~~d) Thermosonde-calculated (black), radiosonde-estimated (blue), and model-estimated (red) C_n^2. The dashed line represents the 3 km minimum for evaluating the error between the profiles. Note that the x axis in panel c) is capped at 0.18 K to show the variability in the temperature differences above 1 km.

DISCUSSION

The radiosonde-estimated C_n^2 obtained from the 5 May 2018 launch agree with the estimated C_n^2 profile calculated from the HRRR forecast sounding. A surprising similarity between the radiosonde and model estimated C_n^2 is the stark agreement in the sharp decrease in C_n^2 near the 3 km level of the 5 May 2018 launch (~~Figure 6~~**c)**. The average logarithmic difference between the radiosonde and model C_n^2 is much smaller than the statistics reported by Frehlich et al;[11] however, the degree that the thermosonde data match the radiosonde data is not as high as anticipated. Previous studies, including Jumper et al.,[16] observed significant variability in C_n^2 data through the entire profile. As seen in ~~Figure 6~~, the general pattern of the thermosonde C_n^2 profile and the radiosonde-estimated C_n^2 profile above 10 km agree, but the amount of variability in the thermosonde data is not as large as that of the smoothed radiosonde C_n^2 profile or of the results found by Frehlich et al. and Jumper et al.[11, 16] Near the 20 km level during the 5 May 2018, there is a large increase in radiosonde-estimated C_n^2 and a smaller increase in thermosonde C_n^2 that agrees with an increase in the radiosonde-estimated C_n^2. Below 10 km, however, there is less similarity between the profiles. Despite the apparent resolution differences between the USIP thermosonde and the thermosondes used in the Frehlich et al. study, as well as the apparent disagreement seen in ~~Figure 6~~, the statistical comparison values from the 5 May 2018 flight thermosonde launch are close to the values reported by Frehlich et al. The average difference in logarithmic C_n^2 in the troposphere is 0.058 +/- 0.628 and for Frehlich et al. study is 0.065 +/- 1.236,[11] which indicates agreement within the standard deviation. For the stratosphere, the average difference in logarithmic C_n^2 is 0.410 +/- 0.441 and for the Frehlich et al. study is 0.116 +/- 0.359.[11] This stratospheric difference are not as comparable as the tropospheric difference; however, the ranges of the two values have a significant overlap which indicate reasonable agreement.

There are a few surprising results from the 5 May 2018 flight. One large surprise is the lack of large-scale variability in both the raw and smoothed thermosonde data. The thermosonde data collected by Frehlich et al. has a large amount of variability from the surface up to 30 km.[11] While the thermosonde data from the 5 May 2018 flight does exhibit some small variability around the average profile, the variability is nowhere near the level of variability seen in the Frehlich et al. paper. This could be due, in part, to slight differences in the make-up of the thermosondes between the USIP project and the project outlined in Frehlich et al. [11] Previous studies involving thermosondes, such as the study by Murphy et al., used 2.5 micron-diameter platinum wires as the thermosonde probes.[12] While the original plan for the USIP project was to use 2.5 micron-diameter platinum wires, 2 micron-diameter platinum wires had to be substituted because of the extreme difficulty in finding 2.5 micron-diameter platinum wires. ~~The same methods for accounting for the resistance differences with the 2.5 micron-diameter wires were applied to the 2 micron-diameter wires, potentially introducing error into the final temperature difference~~ measurements. ~~A possible cause for the lack of variability in the thermosonde data is that the sensitivity is not as high as planned. The differences in platinum wire sizes could affect the sensitivity of the instrument.~~

For the 4 May 2019 flight, the thermosonde signal processing components were reworked to increase the sensitivity of the instrument. The vertical variability in the 4 May 2019 flight thermosonde C_n^2 is significantly higher than in the 54 May 2018 flight although the thermosonde C_n^2 from the second launch does not match as well with the variability in the radiosonde-estimated C_n^2. The increased variability indicates that the changes made to the thermosonde improve the C_n^2 measurements. However, the thermosonde C_n^2 seems to be out of phase with the radiosonde-estimated C_n^2. The exact cause of this out-of-phase relationship is not known. It could be due to problems with the connection between the radiosonde and thermosonde, as features in the radiosonde-estimated profile appear similar to features in the thermosonde profile at lower altitudes.

CONCLUSIONS

A digital thermosonde instrument was developed and built by students at the University of North Dakota. The 5 May 2018 flight of the had thermosonde estimated profiles of C_n^2 from the radiosonde data and a model sounding that agreed very well. While the radiosonde-estimated C_n^2 and the thermosonde C_n^2 do not agree as well, the range of comparison values is consistent with those seen in previous studies. The horizontal temperature differences measured by the thermosonde are close to the vertical temperature differences calculated from the radiosonde data, and significant atmospheric features found in the radiosonde data can also be found in the thermosonde data, which supports the validity of the thermosonde measurements. The observations from the second thermosonde launch conducted on 4 May 2019 showed increased sensitivity to varying optical turbulence through the lower atmosphere, due possibly to the modified signal processing components for the 4 May 2019 flight.

Field Code Changed

Commented [DD2]: Seems to be missing a Figure nuber here.

Commented [DD3]:

Formatted: Highlight

Formatted: Highlight

Formatted: Highlight

Formatted: Highlight

Field Code Changed

Field Code Changed

Commented [DD4]: Did the method include adjusting for the diameter of the wire. If so, then not sure how it would make a difference.

Commented [DD5]: Not sure of the meaning, can you rewrite and improve?

Commented [DD6]: Here you indicate processing component issue for difference in varibility; however above indicated that wire diameter was a reason. Seems like we could just say that it is do to the processing compoent and not the wire. Is this true, if so revise.

Commented [BS7R6]: I modified the text to focus on the changes in processing components rather than the size of the wire.

Commented [DD8]: Nice to include the reason for this improvement here. Improvement in the processing compoents?

AVAILABILITY

All data collected during this project, and used to create the figures within this article, are available in a University of North Dakota online data collection.[17] All programs used for data processing, analysis, and visualization are stored online in the open-source Sourceforge repository for the Airborne Data Processing and Analysis (ADPAA) software packages[15], which is archive via Zenodo.[18]

ACKNOWLEDGEMENTS

This research is part of a NASA-funded Undergraduate Student Instrument Project (USIP). We would like to thank the whole USIP team, which include people from the Space Studies department and the North Dakota Space Grant Consortium. Specifically, we acknowledge help from Dr. Ron Fevig, Dr. Caitlin Milera, Dr. Marissa Saad, and Denise Buckner for organizing the project and planning balloon launches. From the Electrical Engineering department, we acknowledge help from Dr. Naima Kaabouch, Michael Mullins, and Kyle Foerster for building and maintaining the thermosonde for the many tests and launches.

REFERENCES

1. K. W. Fischer, M. R. Witiw, J. A. Baars, and T. R. Oke, "Atmospheric laser communication," *Bull. Am. Meteorol. Soc.*, vol. 85, no. 5, pp. 725–732, May 2004, doi: 10.1175/BAMS-85-5-725.
2. E. M. Dewan, "Optical Turbulence Forecasting: A Tutorial," AIR FORCE GEOPHYSICS LAB HANSCOM AFB MA, AFGL-TR-80-0030, Jan. 1980. Accessed: Mar. 15, 2019. [Online]. Available: https://apps.dtic.mil/docs/citations/ADA086863
3. V. I. Tatarski, *Wave Propogation in a Turbulent Medium*. New York, NY: McGraw-Hill Book Company, Inc., 1961.
4. A. M. Obukhov, "On the Distribution of Energy in the Spectrum of Turbulent Flow," *Dokl. Akad Nauk SSSR*, vol. 32, no. 4, 1941.
5. A. N. Kolmogorov, "Dissipation of Energy in Locally Isotropic Turbulence.," *Dokl. Akad Nauk SSSR*, vol. 32, 1941.
6. J. L. Bufton, "A RADIOSONDE THERMAL SENSOR TECHNIQUE FOR MEASUREMENT OF ATMOSPHERIC TURBULENCE," Goddard Space Flight Center, Greenbelt, Maryland, Technical Note, 1975. [Online]. Available: https://ntrs.nasa.gov/archive/nasa/casi.ntrs.nasa.gov/19750008971.pdf
7. E. M. Dewan, R. E. Good, R. Beland, and J. Brown, "A Model for Csubn(2) (Optical Turbulence) Profiles Using Radiosonde Data," PHILLIPS LAB HANSCOM AFB MA, PL-TR-93-2043, Mar. 1993. Accessed: Mar. 15, 2019. [Online]. Available: https://apps.dtic.mil/sti/citations/ADA279399~~https://apps.dtic.mil/docs/citations/ADA279399~~
8. R. E. Hufnagel, "Propagation Through Atmospheric Turbulence," in *The Infrared Handbook, Ch. 6*, 1978.
9. T. E. Van Zandt, K. S. Gage, and J. M. Warnock, "An Improved Model for the Calculation of Profiles of CN2 and e in the Free Atmosphere from Background Profiles of Wind, Temperature, and Humidity.," presented at the 20th Conference on Radar Meteorology, American Meteorological Society, Boston, MA, 1979.
10. D. J. Richardson, "Solar heating effects on balloon-borne microthermal probes for the airborne laser program," Master's Thesis, Naval Postgraduate School, Monterey, CA, 1997. [Online]. Available: https://calhoun.nps.edu/bitstream/handle/10945/8977/solarheatingeffe00rich.pdf?sequence=1
11. R. Frehlich *et al.*, "Estimates of Cn2 from Numerical Weather Prediction Model Output and Comparison with Thermosonde Data," *J. Appl. Meteorol. Climatol.*, vol. 49, no. 8, pp. 1742–1755, Apr. 2010, doi: 10.1175/2010JAMC2350.1.
12. E. Murphy, P. Tracy, R. Beland, G. Jumper, K. Robinson, and G. Clement, "THERMOSONDE 2007: In-Situ Measurement of Optical Turbulence," Air Force Research Laboratory, Scientific, Final, May 2007. [Online]. Available: https://apps.dtic.mil/sti/citations/ADA551490~~https://apps.dtic.mil/dtic/tr/fulltext/u2/a551490.pdf~~
13. J. Wendell, A. F. Jordan, "iMet-1-RSB Radiosonde XDATA Protocol & Daisy Chaining," *National Oceanic and Atmospheric Administration technical document*. Jan. 2016. [Online]. Available: https://gml.noaa.gov/aftp/user/jordan/iMet-1-RSB%20Radiosonde%20XDATA%20Daisy%20Chaining.pdf
14. A. Krauchi, R. Philipona, G. Romanens, D. F. Hurst, E. G. Hall, and A. F. Jordan, "Controlled weather balloon ascents and descents for atmospheric research and climate monitoring," *Atmospheric Meas. Tech.*, vol. 9, no. 3, pp. 929–938, Mar. 2016, doi: 10.5194/amt-9-929-2016.
15. D. J. Delene, "Airborne data processing and analysis software package," *Earth Sci. Inform.*, vol. 4, no. 1, pp. 29–44, Mar. 2011, doi: 10.1007/s12145-010-0061-4.

16. G. Jumper, J. Vernin, M. Azout, and H. Trinquet, "Comparison of Recent Measurements of Atmospheric Optical Turbulence," in *36th AIAA Plasmadynamics and Lasers Conference*, Toronto, Ontario, Canada, Jun. 2005. doi: 10.2514/6.2005-4778.
17. B. T. Sorenson and D. J. Delene. "Data in 'Development at the University of North Dakota of a Digital Thermosonde Instrument for the Study of Atmospheric Optical Turbulence (C_n^2)"', Dec. 2023. *Datasets*. 29. doi**:** https://doi.org/10.31356/data029. Available: https://commons.und.edu/data/29.
18. Delene, David J., A. Skow, J. O'Brien, N. Gapp, S. Wagner, K. Hibert, K. Sand, and G. Sova, Airborne Data Processing and Analysis Software Package (Version 4267), Zenodo, 22 June 2022, doi:10.5281/zenodo.6685679.

ABOUT STUDENT AUTHORS

Blake Sorenson received a B.S. in Atmospheric Sciences from the University of North Dakota in 2018. He is currently a Ph.D. student in the Atmospheric Sciences program at the University of North Dakota, where he is using remotely-sensed satellite observations to study the radiative impacts of biomass burning aerosols on the Arctic climate and on Arctic sea ice.

PRESS SUMMARY

A NASA Undergraduate Student Instrument Project is building a digital thermosonde instrument to study atmospheric optical turbulence, which is the distortion of light waves by temperature changes in the atmosphere. Optical turbulence makes images of Earth taken from satellites appear wavy and unclear, as well as negatively affecting laser signals moving up through the atmosphere into space. The thermosonde is flown on a high-altitude weather balloon and collects very high-resolution differences in temperature between two fine-wire platinum probes.